Surface-diffusion-driven decay of high-aspect-ratio gratings: Existence of morphologically related classes

Marcos A. Madrid, Roberto C. Salvarezza, and Marcos F. Castez*

Instituto de Investigaciones Fisicoquímicas Teóricas y Aplicadas, UNLP, CONICET, Casilla de Correo 16, Sucursal 4, 1900 La Plata, Argentina

(Received 19 October 2012; revised manuscript received 23 April 2013; published 26 June 2013)

We present numerical and theoretical results concerning the technologically important process of evolution of high-aspect-ratio profiles due to surface diffusion under thermal treatment. We show how a broad class of initial gratings adopt, after a short transient stage, a typical shape that can be accurately described as a curve whose curvature has only two single Fourier modes as a function of the arc-length parameter. Moreover, we introduce a set of evolution equations for the relevant parameters that accounts very accurately for both morphological and kinetic aspects of the transformation processes for these curves in a wide region in parameter space. Regarding the decay of rectangular gratings, our numerical results show the existence of geometrically related classes that asymptotically approach to the same trajectory in parameter space. Gratings belonging to the same class pass through the same sequence of morphologies before reaching the final equilibrium state.

DOI: 10.1103/PhysRevE.87.062407 PACS number(s): 81.10.−h, 68.35.Fx, 62.23.St, 68.60.Dv

I. INTRODUCTION

In the last few years, high-temperature thermal treatments have found new technological applications, particularly in the industry of semiconductors [1–6]. When a high-temperature treatment is applied to a solid sample, it suffers important morphological modifications due to the enhancement of particle mobility. Although different mechanisms, such as evaporation-condensation or bulk diffusion, can contribute to such shape transformation, often, especially in nanoscale applications, surface diffusion is the most important mass-transport process. Surface diffusion processes have attracted considerable interest in several branches of surface science, from both the theoretical and the experimental points of view [3,5,7–9], and important applications of high-temperature thermal annealing have been recently reported to obtain devices with specific photonic or electronic properties. In particular, high-temperature hydrogen annealing has been used on silicon substrates to reduce their surface roughness [1,2], to round trench corners [6], to obtain special topologies [3–5], etc. Regarding the theoretical interpretation of these applications of high-temperature hydrogen annealing to change the morphological properties of semiconductor samples, it is worth remarking that such results have been properly interpreted in terms of the continuous theory of surface diffusion for isotropic materials [2,6,10,11].

The continuous theory of interface evolution mediated by surface diffusion started more than 50 years ago with the pioneering work of Herring and Mullins [12,13]. In this framework, the interface evolution for an isotropic sample is governed by the Mullins equation:

$$v_n = -K\Delta_S \mathcal{C}, \tag{1}$$

where v_n is the normal velocity at a given point on the evolving surface, Δ_S is the intrinsic surface Laplacian (the so-called Laplace-Beltrami operator), and $\mathcal{C}$ is the local curvature. The coefficient K depends both on the type of material considered and on the temperature through the relationship $K = \frac{D_S \gamma \Omega^2 \nu}{k_B T}$, where D_s is the diffusion constant, γ is the surface tension, Ω is the atomic volume, ν is the adatom density on the surface, k_B is the Boltzmann constant, and T is the absolute temperature [14].

When a high-aspect-ratio (HAR) grating decays due to surface diffusion currents, typically the interface adopts a particular sinuous shape that evolves in time. In the case of gratings having an inversion symmetry (the so-called peak-valley symmetry), this particular shape can be accurately described as a curve in which the curvature is a sine function of the arc-length parameter. Such curves were named "sine-generated curves" after Leopold and Langbein [15] introduced them to describe the typical shape found in river meanders. As sine-generated curves are inversion invariant, they cannot be used to describe the morphology of interfaces that do not have this symmetry property. The difference between both situations is clearly shown in Fig. 1, where the shape of the interface is shown at successive times for both cases: the symmetrical one (left side of Fig. 1) and the nonsymmetrical one (right side of Fig. 1).

Performing a detailed study about the kinetic and morphological aspects during the surface-diffusion-driven decay of high-aspect-ratio gratings like that shown on the right side of Fig. 1 is the main goal of this paper. In order to describe the morphology of a general-type grating we will need to generalize the class of sine-generated functions, as we will show in the next section. Such generalization let us describe not only morphological aspects but also kinetic properties of the decaying process.

II. RELEVANCE OF TWO-COMPONENT SINE-GENERATED CURVES

One of the most distinctive features concerning the surface-diffusion-driven decay of one-dimensional HAR gratings is the spontaneous loss of convexity in the evolving interface; i.e., gratings that initially can be thought as the graph of a function $y(x)$ cannot be represented in that way at later times because

*fcastez@inifta.unlp.edu.ar

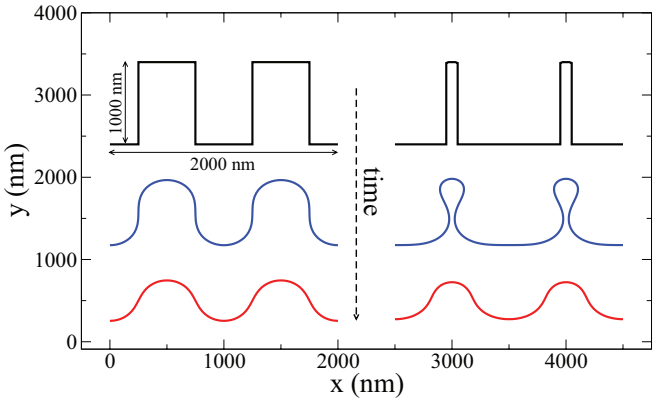

FIG. 1. (Color online) (left) Symmetric and (right) nonsymmetric interfaces and their evolution at successive time steps.

they develop a multivalued character. An alternative approach to describe a plane curve, which can deal perfectly with such multivalued interfaces, is provided by the so-called Whewell equation, in which the interface is described by giving the angle $\theta(s)$ between its tangent and a fixed axis (the x axis, for instance) as a function of the arc-length parameter s. The Whewell equation is an *intrinsic* equation in the sense that it is independent from the choice of the origin of coordinates.

The typical grating on which we are focusing in this paper is a periodic one (with wavelength λ_x) and is disposed along the x axis in the sense that the whole pattern can be obtained by translating, in an amount λ_x and parallel to the x axis, any piece of the grating contained in a length equal to the wavelength. Let us call λ_s the arc length in a period. The grating periodicity evidently implies that $\theta(s)$ is also a periodic function with period λ_s; therefore we can expand it in a Fourier series. Moreover, for gratings having a symmetry axis (as is the case of the gratings in Fig. 1), after a suitable choice of the coordinates origin we can obtain an odd function $\theta(s)$, which contains only sine components in its Fourier expansion:

$$\theta(s) = \sum_{n=1}^{\infty} A_n \sin(nk_s s), \tag{2}$$

where $k_s = \frac{2\pi}{\lambda_s}$. As periodicity and symmetry properties of gratings are preserved by the surface diffusion flow, Eq. (2) remains a valid description for the time-dependent tangential angle $\theta(s,t)$ during the whole decay process, provided coefficients $A_n(t)$ and $\lambda_s(t)$ are time dependent. In fact, although λ_x is a conserved quantity, that is not true for λ_s: an immediate consequence of the Mullins equation is that the total length $L(t)$ of the interface satisfies the following relationship [16]:

$$\frac{dL(t)}{dt} = -K \int_{L(t)} \mathcal{C}_s^2 ds, \tag{3}$$

where $\mathcal{C}_s$ denotes the derivative of the curvature $\mathcal{C}$ with respect to the arc-length parameter. As the right side of Eq. (3) is nonpositive, this equation proves that $\lambda_s(t)$ decreases as time evolves.

In Fig. 2(a) the shape adopted by a HAR interface during the surface-diffusion-driven decay at successive times can be seen. Figure 2(b) shows the dependence of the curvature as a function of the arc-length parameter corresponding to each

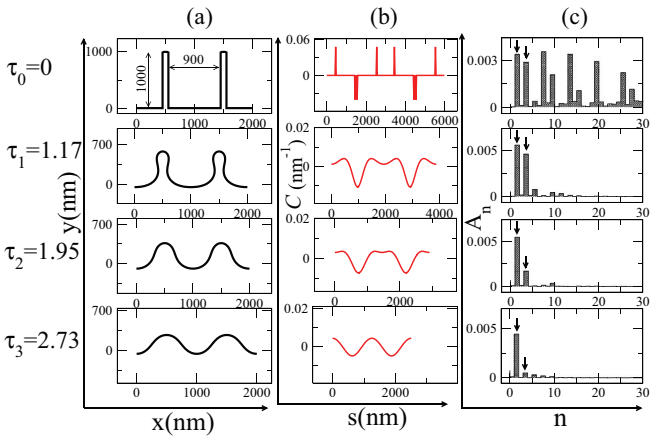

FIG. 2. (Color online) (a) Interface profile snapshots at different times. (b) Curvature as a function of the arc length parameter. (c) Fourier coefficient A_n as a function of index n (the arrows indicate components $n = 1$ and $n = 2$). In all cases, the shown data correspond to the state at the initial stage (τ_0) and at three successive stages labeled τ_1,τ_2, and τ_3.

interface shown in Fig. 2(a). It is clear from this graph that, in contrast to what happens with gratings having the peak-valley symmetry, profiles at intermediate stages (τ_1 and τ_2) are not single sine functions of the arc parameter. In Fig. 2(c) Fourier coefficients A_n for the first harmonics are shown as a function of the index n. While many components are relevant at the initial stage (τ_0), after a brief period of time only the first two components contribute significantly (τ_1,τ_2). Later on the second component becomes negligible, only the first one survives (τ_3) and the interface profile becomes symmetric. This analysis suggests that the appropriate Whewell equation to describe the class of interfaces appearing after the initial transient stage ($\tau_0 - \tau_1$) [17] should have two components, leading us to the following equation:

$$\theta(s) = A_1 \sin(k_s s) + A_2 \sin(2k_s s). \tag{4}$$

The described behavior is not restricted to the case of initially rectangular profiles. In fact, as is shown in Fig. 3, there are a wide variety of morphologically different patterns that,

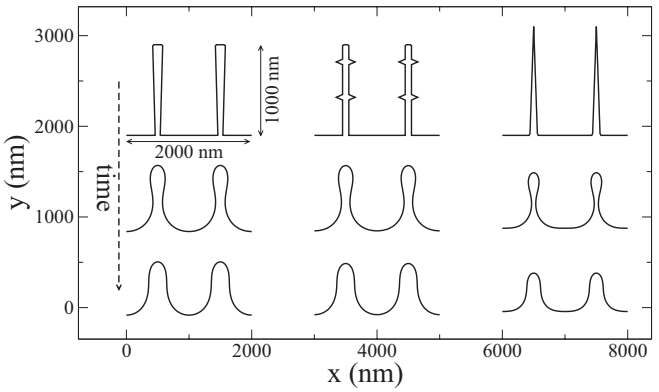

FIG. 3. Decay of different HAR pattern classes (trapezoidal, distorted rectangular, and triangular) at successive times, exhibiting a very similar morphology after an initial transient stage has elapsed.

after a short transient stage, adopt nearly the same morphology found for initially rectangular profiles (see Fig. 3).

The Whewell equation $\theta = \theta(s)$ implies the following differential forms for the x and y components:

$$dx = \cos[\theta(s)]ds \tag{5}$$

and

$$dy = \sin[\theta(s)]ds, \tag{6}$$

and combining these equations with the Whewell equation (4), we can find parametric equations for the x and y components as functions of the arc-length parameter:

$$x(s) = \int_0^s \cos[A_1 \sin(k_s u) + A_2 \sin(2k_s u)]du + x_0 \tag{7}$$

and

$$y(s) = \int_0^s \sin[A_1 \sin(k_s u) + A_2 \sin(2k_s u)]du + y_0. \tag{8}$$

It is evident that the x component increases from x to $x + \lambda_x$ when the arc-length parameter increases in a period λ_s, which allows us to obtain λ_x as a function of parameters A_1, A_2, and λ_s as

$$\lambda_x = \int_0^{\lambda_s} \cos[A_1 \sin(k_s u) + A_2 \sin(2k_s u)]du. \tag{9}$$

Applying elementary trigonometric relationships and performing suitable changes of variables in Eq. (9), after combining with the identities associated with the Bessel functions [18],

$$\cos[z \sin(\theta)] = J_0(z) + 2\sum_{n=1}^{\infty} J_{2n}(z)\cos(2n\theta), \tag{10}$$

$$\sin[z \sin(\theta)] = 2\sum_{n=0}^{\infty} J_{2n+1}(z)\cos[(2n+1)\theta], \tag{11}$$

we can obtain

$$\lambda_x = \lambda_s F(A_1, A_2), \tag{12}$$

where

$$F(A_1, A_2) = J_0(A_1)J_0(A_2) + 2\sum_{n=1}^{\infty} J_{4n}(A_1)J_{2n}(A_2), \tag{13}$$

while J_i represents the Bessel function of the first kind and order i.

To perform a quantitative estimation of the order of magnitude of the transient time in a typical case we will consider a simulation regarding the decay of a HAR rectangular grating whose initial shape is shown in the inset in the left panel in Fig. 4. The time evolution of $\frac{\lambda_s}{\lambda_x} - 1$ is shown in the left panel in Fig. 4 [19]; evidently, this quantity tends to zero asymptotically as the interface approaches the equilibrium flat shape. So we can estimate the overall decaying time τ_d defining it as the time at which the value of $\frac{\lambda_s}{\lambda_x} - 1$ is a 10% of its initial value. On the other hand, we will estimate the magnitude of the transient time applying the Bessel-Parseval relationship to the curvature function $\mathcal{C}(s)$. In fact, as $\mathcal{C} = \frac{d\theta}{ds}$, Eq. (4) implies that the curvature of such a curve is given by

$$\mathcal{C}^{(a)} = C_1 \cos(k_s s) + C_2 \cos(2k_s s), \tag{14}$$

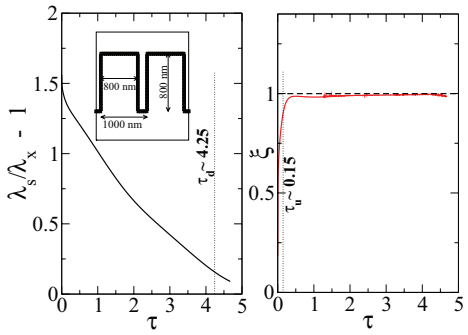

FIG. 4. (Color online) Time dependence of (left) $\frac{\lambda_s}{\lambda_x} - 1$ and (right) ξ obtained from a simulation started with the initial condition shown in the inset on the left panel. The meanings of ξ, τ_d, and τ_u are explained in the text.

where $C_1 = k_s A_1$ and $C_2 = 2k_s A_2$ [20]. Defining $\xi = \frac{C_1^2 + C_2^2}{\frac{2}{\lambda_s}\int_0^{\lambda_s} \mathcal{C}^2(u)du}$, the Bessel-Parseval inequality ensures that $\xi \leqslant 1$, so the two-harmonics approximation will be considered as "good" when $\xi \geqslant 0.9$. The time dependence of ξ is shown in the right panel of Fig. 4. We can see that ξ grows monotonically until values near 1; we shall call τ_u the time at which ξ reaches the value 0.9. Both τ_d and τ_u are indicated with dashed lines in Fig. 4; considering these values, we notice that τ_u represents approximately 3.5% of τ_d, in agreement with our previous observation that the transient stage is rather short compared with the overall process.

It should be noticed that not every parameter choice of A_1 and A_2 in Eq. (4) gives place to a physically realistic interface (i.e., a curve representing a real grating). For instance, when $A_2 = 0$ and $|A_1|$ is higher than $\sim$2.11, the resulting curve self-intercepts, leading to nonphysical curves. From now on we shall only consider parameter values belonging to the region in parameter space where the resulting curves become physically realistic (in the sense that they do not present self-intersections). Such a region in parameter space, numerically determined, is shown in Fig. 5.

III. EVOLUTION EQUATIONS FOR THE PARAMETERS OF TWO-COMPONENT SINE-GENERATED CURVES

As was stated in the previous section, numerical evidence shows that a HAR grating develops, under a surface diffusion

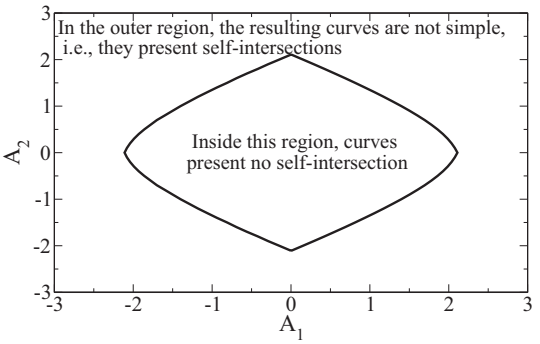

FIG. 5. Region in parameter space where the Whewell equation (4) generates physically realistic interfaces for two-component sine-generated curves.

flow and after a transient stage has elapsed, a typical shape that can be accurately described as a two-component sine-generated curve (2CSGC). Moreover, numerical evidence also shows that once the interface adopts that shape, it maintains it for the rest of the decaying process. As the knowledge of the values of parameters A_1, A_2, and λ_s is enough to define uniquely a 2CSGC, it is clear that knowing the time dependence of such parameters will allow us to reproduce the shape of the interface at any time during its evolution. To obtain a closed system of evolution equations for the parameters, we would need three relationships involving time derivatives of $A_1(t)$, $A_2(t)$, and $\lambda_s(t)$.

A first relationship can be obtained using the fact that the surface diffusion flow preserves the periodic nature of the interface. Thus, imposing periodic boundary conditions on the Mullins equation, we look for periodic solutions in which λ_x remains fixed at the time, and therefore Eq. (12) can be written as

$$\lambda_s(t) = \frac{\lambda_x}{F(A_1(t), A_2(t))}. \tag{15}$$

Equation (15) tells us that for a fixed value of λ_x, knowing the time dependence of coefficients A_1 and A_2, we can obtain the time dependence of λ_s. Differentiating Eq. (15) with respect to t and using $2J_n'(z) = J_{n-1}(z) - J_{n+1}(z)$, we obtain

$$\frac{d\lambda_s}{dt} = -\frac{\lambda_s^2}{\lambda_x}\Big\{-J_1(A_1)J_0(A_2)A_1' - J_0(A_1)J_1(A_2)A_2' + \sum_{j=1}^{\infty}[J_{2j-1}(A_2)J_{4j}(A_1)A_2' + J_{2j}(A_2)J_{4j-1}(A_1)A_1' - J_{2j+1}(A_2)J_{4j}(A_1)A_2' - J_{2j}(A_2)J_{4j+1}(A_1)A_1']\Big\}, \tag{16}$$

where A_i' denotes the derivative of $A_i(t)$ with respect to t.

A second relationship among coefficients can be obtained by evaluating Eq. (3) in a period of a 2CSGC. In such a case, $L(t) = \lambda_s(t)$, and using $\theta_{ss} = \mathcal{C}_s$, Eq. (3) becomes

$$\frac{d\lambda_s}{dt} = -8K\pi^4\left(\frac{A_1^2(t) + 16A_2^2(t)}{\lambda_s^3(t)}\right). \tag{17}$$

On the other hand, we can obtain a third relationship among coefficients by writing down the Mullins equation in terms of $\theta(s,t)$ (see the paper by Asvadurov *et al.* [21] for a detailed derivation):

$$\theta_{ss}\theta_t - \theta_s\theta_{ts} = K\left(\theta_s\theta_{sssss} - \theta_{ss}\theta_{ssss} + \theta_s^3\theta_{sss}\right). \tag{18}$$

Replacing in Eq. (18) the expression of $\theta(s,t)$ for a 2CSGC (4), we obtain

$$\begin{aligned}
&-2k_s^2\Big\{A_1A_1' + A_1A_2'[\sin(k_ss)\sin(2k_ss) + \cos(k_ss)\cos(2k_ss)] - A_1^2\frac{1}{\lambda_s}\frac{d\lambda_s}{dt}\cos^2(k_ss) - 4A_1A_2\frac{1}{\lambda_s}\frac{d\lambda_s}{dt}\cos(k_ss)\cos(2k_ss)\\
&\quad + A_2A_1'[4\sin(k_ss)\sin(2k_ss) + 2\cos(k_ss)\cos(2k_ss)] + 4A_2A_2' - 4A_2^2\frac{1}{\lambda_s}\frac{d\lambda_s}{dt}\cos^2(2k_ss)\Big\}\\
&= Kk_s^6\{A_1^2 + 64A_2^2 + A_1A_2[34\cos(k_ss)\cos(2k_ss) + 20\sin(k_ss)\sin(2k_ss)] - A_1^4\cos^4(k_ss) - 64A_2^4\cos^4(2k_ss)\\
&\quad -14A_1^3A_2\cos^3(k_ss)\cos^2(2k_ss) - 60A_1^2A_2^2\cos^2(k_ss)\cos^2(2k_ss) - 104A_2^3A_1\cos^3(2k_ss)\cos(k_ss)\}.
\end{aligned} \tag{19}$$

From this equation, we can conclude that 2CSGCs are *not* exact solutions of the Mullins equation since we cannot eliminate the parameter s, which contradicts our assumption that parameters A_1, A_2, and λ_s are not dependent on s. However, numerical simulations show that they are very good approximations to such exact solutions. To reconcile these facts, we will perform an averaging procedure to obtain an approximated equation for $\frac{d\lambda_s}{dt}$. The motivation for such an averaging procedure is the following: we are attempting to find an expression for $\frac{d\lambda_s}{dt}$ that is a global quantity, so we argue that the overall contribution of terms dependent on s in Eq. (19) can be approximated by replacing local values (i.e., dependent on s) with values averaged in one period. Here we are understanding the averaging of functions in the ordinary sense of calculus: $\langle f\rangle = \frac{1}{\lambda_s}\int_0^{\lambda_s} f(s)ds$. Applying this procedure, we obtain

$$\begin{aligned}
\frac{d\lambda_s}{dt} &= \left\langle\frac{d\lambda_s}{dt}\right\rangle\\
&= \frac{2\lambda_s}{A_1^2(t) + 4A_2^2(t)}\left\{A_1(t)A_1'(t) + 4A_2(t)A_2'(t) + Kk_s^4\left[A_1^2(t) + 64A_2^2(t) - \frac{3}{8}A_1^4(t) - 24A_2^4(t) - 15A_1^2(t)A_2^2(t)\right]\right\}.
\end{aligned} \tag{20}$$

Then, eliminating $\frac{d\lambda_s}{dt}$ from Eqs. (15), (17), and (20) and introducing the definitions

$$P(A_1,A_2) = -J_1(A_1)J_0(A_2) + \sum_{n=1}^{\infty}J_{2n}(A_2)[J_{4n-1}(A_1) - J_{4n+1}(A_1)], \tag{21}$$

$$Q(A_1,A_2) = -J_0(A_1)J_1(A_2) + \sum_{n=1}^{\infty}J_{4n}(A_1)[J_{2n-1}(A_2) - J_{2n+1}(A_2)], \tag{22}$$

$$O(A_1,A_2) = k_s^4\left(\frac{1}{8}A_1^4 + 8A_2^4 + 10A_1^2A_2^2 - A_1^2 - 64A_2^2\right), \tag{23}$$

$$T(A_1,A_2) = \frac{1}{2}k_s^4\left(A_1^2 + 16A_2^2\right)F(A_1,A_2) \tag{24}$$

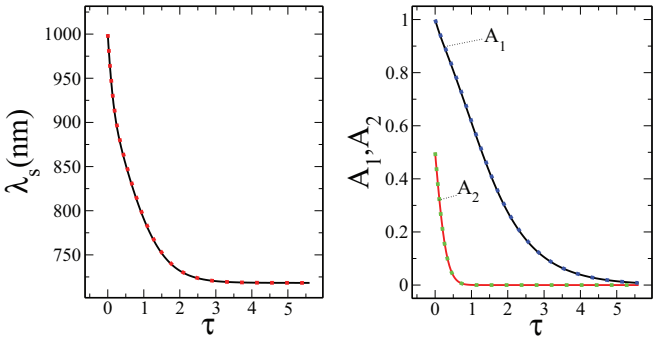

FIG. 6. (Color online) Comparison between analytical predictions (dashed lines) and numerical results (solid lines) regarding the time evolution of (left) λ_s and (right) A_i for a 2CSGC with parameters $\lambda_s = 1000$ nm, $A_1 = 1.0$, and $A_2 = 0.5$ at the initial condition.

to lightening the notation, we obtain the following evolution equations for parameters A_1 and A_2:

$$A_1'(t) = K\left(\frac{OQ - 4TA_2}{QA_1 - 4PA_2}\right) \tag{25}$$

and

$$A_2'(t) = K\left(\frac{TA_1 - PO}{QA_1 - 4PA_2}\right). \tag{26}$$

Equations (25) and (26) taken in conjunction with Eq. (15) form a complete set of evolution equations for 2CSGC relevant parameters. Given that we have used the approximation established in Eq. (20), this set of evolution equations must be also understood as an approximation of the real evolution. To test the ability of this approximated scheme to reproduce the actual evolution, we have contrasted theoretical predictions against direct numerical integrations of the Mullins equation for a wide range of initial gratings. Thus, for an initial 2CSGC with parameters values $A_1 = 1.0$ and $A_2 = 0.5$, Fig. 6 shows excellent agreement between the numerical simulation (solid lines) and theoretical expectations (dashed lines). Similarly, we have found also a very good agreement between theoretical and numerical results for several cases in which the initial values of parameters A_1 and A_2 were restricted to the range ($\sim$0.5, $\sim$1.0). However, in cases in which one of these parameters has a smaller initial value, the differences between theoretical and numerical results increase dramatically. For instance, this behavior can be seen in Fig. 7, where initial values of parameters were taken to be $A_1 = 1.5$ and $A_2 = 0.1$.

To understand the origin of this singular behavior (the approximation gets poorer when one of the parameters approaches zero [22]) we must study what the behavior of the denominator $(QA_1 - 4PA_2)$ in Eqs. (25) and (26) is for values of the parameters near the origin. In fact, from a simple Taylor expansion, we obtain (at the lowest order) $(QA_1 - 4PA_2) \sim \frac{3}{2}A_1A_2$, which implies that the factor A_1A_2 should be present in all terms in the numerator of Eqs. (25) and (26) to produce a nonsingular behavior. In particular, the presence of terms containing just one of parameters A_1 and A_2 will carry a singular contribution to evolution equations (25) and (26). By performing Taylor expansions in both numerators $(OQ - 4TA_2)$ and $(TA_1 - PO)$ we can verify that this is precisely the case: due to the approximation introduced

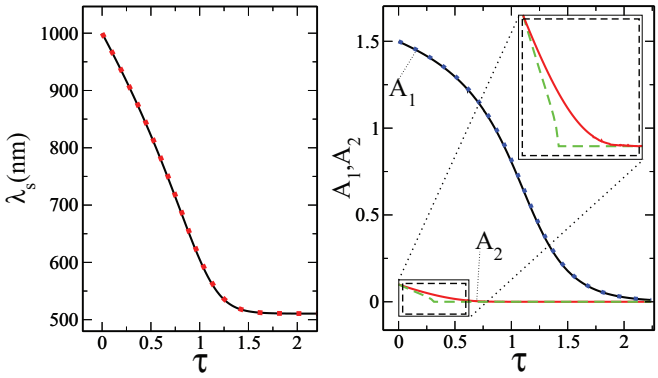

FIG. 7. (Color online) Comparison between analytical predictions (dashed lines) and numerical results (solid lines) regarding the time evolution of (left) λ_s and (right) A_i for a 2CSGC with parameters $\lambda_s = 1000$ nm, $A_1 = 1.5$, and $A_2 = 0.1$ at the initial condition. It can be seen that curves corresponding to parameter A_2 have a very different behavior when $A_2 \to 0$.

in Eq. (20) $OQ - 4TA_2$ contains a singular term $C_1(A_2)$, while $TA_1 - PO$ contains a singular term $C_2(A_1)$, whose expressions are

$$C_1(A_2) = -8\left(\frac{2\pi}{\lambda_x}\right)^4 J_0^4(A_2)A_2^2 \times \left[4A_2J_0(A_2) + J_1(A_2)\left(A_2^2 - 8\right)\right] \tag{27}$$

and

$$C_2(A_1) = \frac{1}{2}\left(\frac{2\pi}{\lambda_x}\right)^4 J_0^4(A_1)A_1^2 \times \left[A_1J_0(A_1) + 2J_1(A_1)\left(\frac{1}{8}A_1^2 - 1\right)\right]. \tag{28}$$

Evidently, to obtain a set of evolution equations having the right behavior when parameters approach the origin, we must eliminate these singular terms from Eqs. (25) and (26), so we will rewrite these equations in the following way:

$$A_1'(t) = K\left(\frac{OQ - 4TA_2 - C_1(A_2)}{QA_1 - 4PA_2}\right), \tag{29}$$

$$A_2'(t) = K\left(\frac{TA_1 - PO - C_2(A_1)}{QA_1 - 4PA_2}\right). \tag{30}$$

We have reperformed the comparison between theoretical and numerical results for an initial 2CSGC with $A_1 = 1.5$ and $A_2 = 0.1$ using the corrected set of evolution equations (29) and (30). As can be seen in Fig. 8 the agreement is excellent, and the singular behavior has been removed. Further results of the performance of these analytical findings in describing the actual kinetic properties of the decay process are given in the following section.

IV. NUMERICAL RESULTS

Once we obtain the set of evolution equations (29) and (30), it is worth comparing the predicted evolution with the real evolution. Here, we are calling the "real evolution" the one obtained by a direct numerical integration of the Mullins equation (1). In particular, due to the approximate nature of

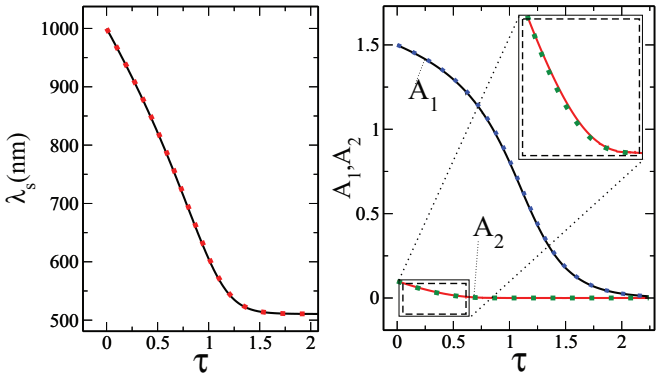

FIG. 8. (Color online) Time-evolution of (left) λ_s and (right) A_i, using the corrected set of equations (29) and (30) (dashed lines) and those obtained from a numerical integration of Mullins equation (solid lines). The initial interface is a 2CSGC with parameters $\lambda_s = 1000$ nm, $A_1 = 1.5$ and $A_2 = 0.1$.

evolution equations (29) and (30), we need to establish in which cases the approximation is accurate. For instance, in Fig. 9 we compare the evolution resulting from three different 2CSGCs as initial conditions that have the same initial value $\lambda_s = 1000$ nm [initial values for the remaining parameters are $A_1 = 1.0$ and $A_2 = 0.3$ (Fig. 9, row I), $A_1 = 1.3$ and $A_2 = 0.5$ (Fig. 9, row II), and $A_1 = 1.5$ and $A_2 = 0.6$ (Fig. 9, row III)]. The agreement between predicted and real evolutions is excellent, as curves obtained with both approaches are almost indistinguishable. It is important to stress that such an agreement was found in cases in which the initial interface has extremely high-aspect-ratio features and a manifest lack of peak-valley symmetry, as can be seen considering the initial interfaces shown in Fig. 9, column (c).

Looking closely at the case with initial values of $A_1 = 1.5$ and $A_2 = 0.6$, we can observe small deviations between both approaches (Fig. 10, left). To obtain a quantitative measure of these errors in a typical case, we can consider the evolution

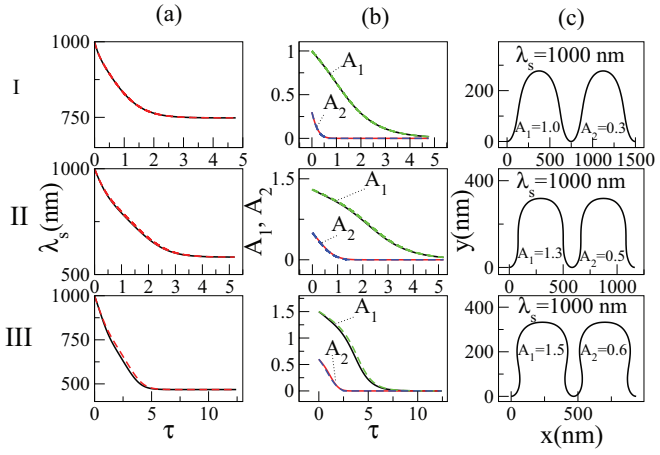

FIG. 9. (Color online) Time evolution of λ_s [column (a)] and A_i [column (b)] using the corrected set of equations (29) and (30) (dashed lines) and those obtained from a numerical integration of the Mullins equation (solid lines) for three different HAR initial conditions, rows I, II, and III [snapshots and parameter values of the initial profiles are shown in column (c)].

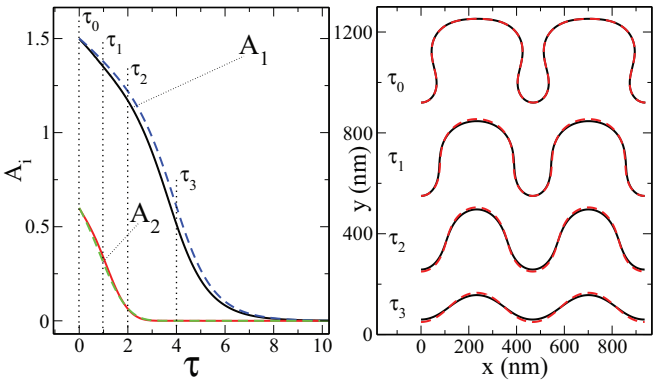

FIG. 10. (Color online) Correlation between differences in (left) $A_i(\tau)$ and (right) their associated profiles for numerical simulations (solid lines) and theoretical predictions (dashed lines). The initial parameters of the 2CSGC are $\lambda_s = 1000$ nm, $A_1 = 1.5$, and $A_2 = 0.6$. Curves corresponding to different values of τ (on the right) are displaced along the y axis for easy viewing.

of parameter A_1 in the left panel of Fig. 10, which represents the case (among all comparative curves shown in this paper) having the poorest fitting: for that curve, the relative error at times labeled τ_1, τ_2, and τ_3 are 2.1%, 4.2%, and 18.2%, respectively. Considering such differences, one might ask how they impact the morphological point of view. This question is addressed if we consider the snapshots in the right panel of Fig. 10, where we can see that the interface's morphologies associated with instantaneous values of parameters $A_i(\tau)$ are almost identical for both approaches.

We are not attempting in this paper an exact determination of the boundaries of the region where the set of equations (29) and (30) reproduces the results obtained from a direct integration of the Mullins equation for initial conditions of type 2CSGC. However, after performing such comparative work sampling different points in parameter space, we have found that, as a rule of thumb, for initial parameters satisfying $|A_1| \lesssim 1.5$ and $|A_2| \lesssim 0.6$ the agreement between both approaches is very good, typically with relative errors in the range of 1%–5%. As the linear equation for surface diffusion is reobtained when $(A_1, A_2) \to (0,0)$, the performance of the approximated equations in this limit is expected to be (and was corroborated numerically) very close to the real evolution. Beyond this region, errors are more significant, so an increase in the initial parameter values causes a loss of accuracy in the theoretical predictions for the kinetic evolution. To study such cases, we must restrict our analysis to numerical integrations of the Mullins equation.

To move a step forward in the comprehension of the decaying process, we will analyze evolution trajectories in the parameter space (A_1, A_2). As such trajectories are invariant against scale changes (i.e., they are independent of λ_x), a point on this space uniquely identifies a characteristic morphology of 2CSGC. Figure 11 shows trajectories for various 2CSGC (dashed lines) as initial conditions (initial points are indicated by circles). It can be seen that parameter A_2 decays faster than A_1, indicating that a 2CSGC becomes symmetric faster than the time it takes to reduce its amplitude. The trajectory shown in Figure 11 with a solid line corresponds to a rectangular

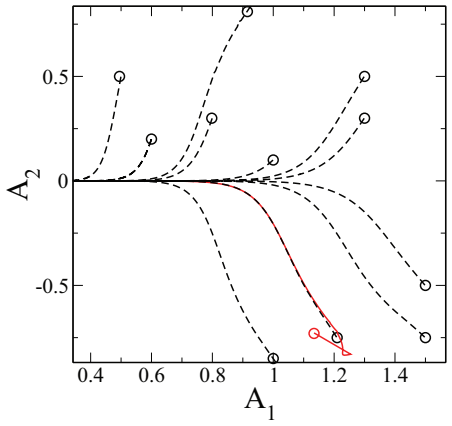

FIG. 11. (Color online) Several trajectories in (A_1, A_2) space for different 2CSGCs as initial conditions (initial values of the parameters are indicated by circles). The trajectory indicated with a solid line corresponds to a rectangular HAR grating as the initial condition.

HAR grating as the initial condition [23]. Such a trajectory shows an initial loop associated with the transient stage, while the remaining part has the same qualitative behavior as the rest of trajectories in Fig. 11, consistent with the fact that after the initial transient stage the grating evolves like a 2CSGC. Let us consider an initial rectangular grating consisting of a periodic arrangement (with a period λ_x) of columns of height H and width T. Considering the behavior in parameter space shown in Fig. 11, a natural question arises: Is it possible to find two such gratings having columns with different dimensions [e.g., (H_1, T_1) and (H_2, T_2)] whose associated trajectories in parameter space become, after the transient stage, a single trajectory? Figure 12 shows that the answer for such a question is affirmative: In Fig. 12(a) we can see three trajectories labeled I, II, and III, and clearly, trajectories II and III merge after a first transient, while trajectory I follows a different path. The initial conditions associated with trajectories I, II, and III are shown in Fig. 12(b), where we have annotated the aspect ratio ε (defined as the ratio $\frac{H_i}{T_i}$) of the columns for

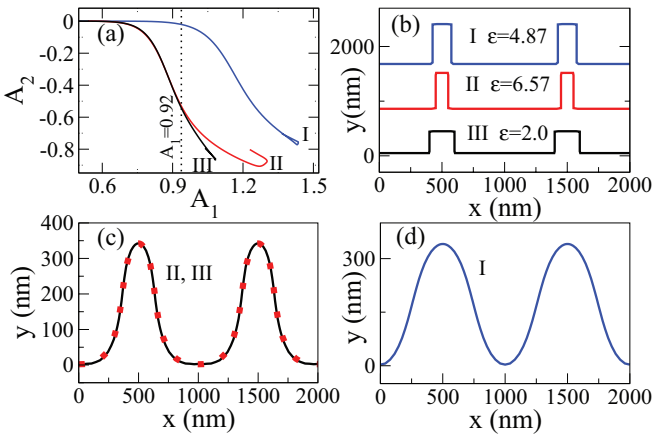

FIG. 12. (Color online) (a) Trajectories on the parameter space (A_1, A_2) for three initial conditions (labeled I, II, and III). (b) Initial gratings. (c) and (d) Shapes adopted by interfaces I, II, and III when the corresponding trajectories cross the dashed line in (a), i.e., when $A_1 = 0.92$.

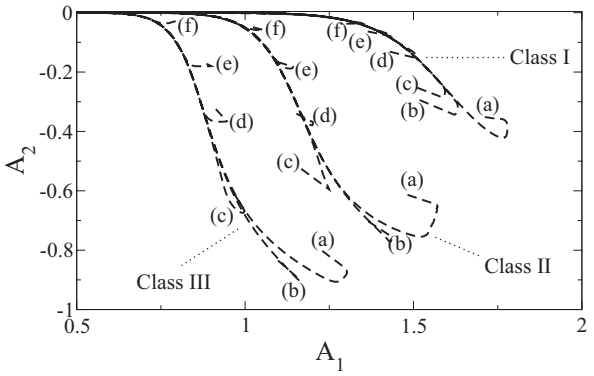

FIG. 13. Collapse of trajectories in parameter space for different initial rectangular gratings, allowing the identification of three particular morphological classes. Specific parameters of the initial conditions are given in Table I.

each grating, showing that, despite the coalescence between its respective trajectories, gratings II and III have very different HAR features from a quantitative point of view. Moreover, if we plot snapshots corresponding to the same value of A_1, for instance, that shown with a dotted line in Fig. 12(a), we obtain nearly the same interface from trajectories II and III [Figure 12(c)], while a very different, much more symmetrical interface is obtained from trajectory I [Fig. 12(d)].

Extending this result to the case of more than two curves, the existence of *classes* or *families* of rectangular gratings that, after the transient stage has elapsed, share the same trajectory on the (A_1, A_2) parameter space becomes evident. We shall call these classes *morphological classes*. Thus, starting from an arbitrary curve in the (A_1, A_2) parameter space, we numerically found a considerable set of different rectangular initial gratings, whose trajectories in this space quickly collapse (see Fig. 13 and Table I). This implies that any pair of these curves with different initial shapes will pass through the same morphologies (for different times each, of course) after the first transient stage has elapsed. Roughly speaking, we can say that, after a given time (which is different for each grating), two gratings belonging to the same morphological class "show the same movie."

To get a deeper understanding of the nature of these classes, we will study the asymptotic behavior of trajectories in (A_1, A_2) space when $(A_1, A_2) \to (0,0)$, considering the corresponding limit form of the analytical coupled equations

TABLE I. Values for heights H and widths T of the columns of the rectangular gratings (in nm) used as initial conditions for the trajectories shown in Fig. 13. $\lambda_x = 1000$ nm in all cases.

	Class I		Class II		Class III	
	T	H	T	H	T	H
(a)	200	1350	100	1000	100	657
(b)	350	797	150	730	150	490
(c)	389	717	320	430	300	302
(d)	450	590	395	370	400	250
(e)	475	520	450	330	450	227
(f)	490	450	485	290	490	97

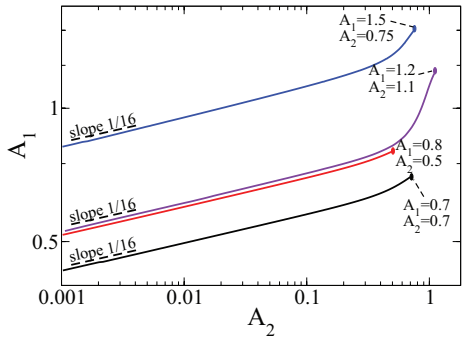

FIG. 14. (Color online) Several trajectories in $(A1, A2)$ space (on a double-logarithmic scale) for different 2CSGCs as initial conditions (initial values of the parameters are indicated for each trajectory).

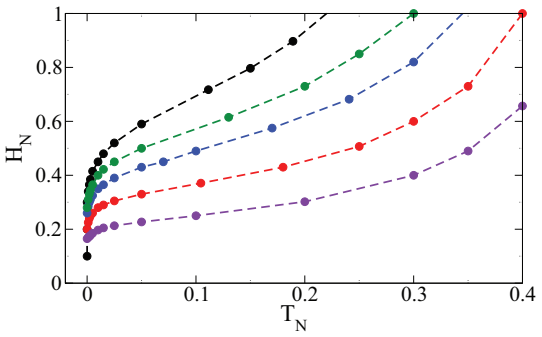

FIG. 15. (Color online) Rectangular HAR gratings with normalized parameters H_n and T_n lying on the same curve belong to the same morphological class. Data indicated with circles were obtained numerically, and dashed lines were drawn by joining points associated with the same class.

[(29) and (30)] discussed in the previous section. In fact, computing the quotient between equations [(29) and (30)], we can eliminate the explicit dependence on the time variable and thus obtain the following differential equation to describe (in an approximated sense) the trajectories in (A_1, A_2) space:

$$\frac{dA_1}{dA_2} = \frac{OQ - 4TA_2 - C_1(A_2)}{TA_1 - PO - C_2(A_1)} . \tag{31}$$

Expanding both the numerator and denominator on the right side of Eq. (31) in powers of A_1 and A_2 and by keeping only the leading terms, we obtain

$$\frac{dA_1}{dA_2} \simeq \frac{1}{16}\frac{A_1}{A_2}. \tag{32}$$

The simplified differential equation (32) captures the behavior of the trajectories in parameter space in the asymptotic limit $(A_1, A_2) \to (0,0)$. Moreover, Eq. (32) can easily be integrated, having the following general solution:

$$A_1 = C|A_2|^{\frac{1}{16}} . \tag{33}$$

Thus, in this limit, trajectories in (A_1, A_2) space can be labeled by the continuous coefficient C. Since Eq. (33) is derived from an approximation, we compared its predictions with numerical simulations, starting from different points in (A_1, A_2) space; the results of such a comparison are given in Fig. 14. The scaling properties for all numeric trajectories shown in Fig. 14 on a log-log scale are fully consistent with the approximated dependence established by Eq. (33).

Concerning the decay of rectangular gratings, a given grating with parameters (H, T) can be associated with a certain asymptotic trajectory labeled by C, but this grating is not the only one associated with such a trajectory: there is an infinite set of gratings (H', T'), (H'', T''), etc., that have the same asymptotic trajectory. All of them belong to the same morphological class. On the other hand, there are an infinite number of morphological classes, a different one for each value of the continuous coefficient C.

From a practical point of view, it would be desirable to know, at least approximately, to which of these morphological classes a given rectangular HAR grating with period λ_x and columns with height and width H and T, respectively, belongs. It will be convenient to introduce the normalized height $H_N = H/\lambda_x$ and width $T_N = \frac{T - \frac{\lambda_x}{2}}{\lambda_x}$, with $0 \leqslant T \leqslant \lambda_x$ (the term $\frac{\lambda_x}{2}$ makes $T_N = 0$ for a grating with peak-valley symmetry). In this sense, we have performed extensive numerical simulations to identify gratings belonging to the same class, complementing the results shown in Fig. 13. So curves in Fig. 15 represent, in terms of the normalized parameters H_N and T_N, the dimensions of initial rectangular gratings that belong to the same class. As gratings with normalized parameters $(H_N, -T_N)$ are related to those with parameters (H_N, T_N) through a reflection in the y axis plus a suitable translation, it is enough to consider only positive values of the normalized width T_N, and data in Fig. 15 can be extended to negative values of T_N as an even function, i.e., symmetrically with respect to the H_N axis. Considering a specific situation, if we have an initial rectangular grating with parameters λ_x, H, and T, we can compute the normalized parameters H_N and T_N; then using Fig. 15, we will be able to estimate the class to which our system belongs. Knowing the morphological class to which a system belongs give us *a priori* information (i.e., before performing the thermal treatment) on which kinds of morphologies can and cannot be obtained during a thermal treatment on such a sample.

V. SUMMARY AND CONCLUDING REMARKS

In this paper we have shown how the morphologies obtained from the surface diffusion decay of a broad class of HAR gratings can be expressed after a short transient time as two-component sine-generated curves with time-dependent parameters. By means of an analytical study and making a few approximations, we have arrived at a set of evolution equations for such parameters. After an extensive comparison with numerical results, we have verified that this set of evolution equations (29) and (30) provides a very accurate description of the kinetic evolution for a broad class of HAR gratings, in situations very far from the conditions in which the linear theory of surface diffusion (the so-called small-slopes approximation) is applicable. By means of this set of evolution equations, we have switched from a system that ordinarily requires a few hundred degrees of freedom (through the discretization of the interface for its numerical integration)

to a system with only two degrees of freedom (parameters A_1 and A_2). Although such a set of coupled equations is too involved to be amenable to a complete analytical solution, by analyzing its limit form when A_1 and A_2 are small enough, we have been able to obtain the asymptotic dependence of curves describing the surface-diffusion-driven decay process in the parameter space (A_1, A_2).

While in some related previous papers [24–27] we employed a parametric explicit description of the interfaces, in this paper we based our analysis on the use of generalized sine-generated functions in conjunction with a description of the interfaces by means of the associated Whewell equation. Such a procedure becomes more natural and gives a much more accurate description of kinetic properties compared with the earlier approach, as was already discussed in Ref. [28]. On the other hand, while Ref. [28] considered only a restricted class of interfaces (i.e., those with peak-valley symmetry), in this paper we considered a broader class of interfaces without such symmetry being prerequisite. In fact, many of the results published in Ref. [28] can be considered as a particular case of the results presented in this paper, taking $A_2 = 0$. However, it is worth noticing that the passage from the one-dimensional parameter space (A_1) to the two-dimensional space (A_1, A_2) is not a trivial one: while in a one-dimensional space there is a single trajectory going from a given point $A_1 \neq 0$ to $A_1 = 0$, in the two-dimensional space there is a rich variety of possible trajectories, and the available routes towards the equilibrium state $(A_1 = 0, A_2 = 0)$ are far from trivial.

By means of a systematic study of the behavior of trajectories in parameter space, we have shown the existence of rectangular HAR gratings with different geometrical dimensions whose trajectories merge after an initial transient stage has elapsed. This fact let us define classes of morphologically related gratings in the sense that two gratings belonging to the same class will have, after a certain time, nearly the same shape. Conversely, a given pattern with a shape described by a two-component sine-generated curve can be obtained by performing a thermal treatment over a rich variety of initial rectangular gratings that belong to the same morphological class.

The grouping of HAR rectangular gratings into morphologically related classes can be useful in applications of high-temperature annealing techniques over HAR gratings and can be helpful in the design and optimization of experiments in this field since it provides *a priori* knowledge on which types of morphologies can and cannot be obtained during the surface diffusion decay process starting from a given sample. We expect this work to promote further experimental research on this topic.

ACKNOWLEDGMENTS

This work has been accomplished as part of projects PICT 2010-2554 and PICT 2010-1921 of ANPCyT (Argentina). We acknowledge support from CONICET (Argentina National Research Council).

[1] R. Hiruta, H. Kuribayashi, S. Shimizu, K. Sudoh, and H. Iwasaki, Appl. Surf. Sci. **237**, 63 (2004).
[2] M.-C. Lee and M. Wu, J. Microelectromech. Syst. **15**, 338 (2006).
[3] M. Bopp, P. Coronel, J. Bustos, C. Pribat, P. Dainesi, T. Skotnicki, and A. Ionescu, Microelectron. Eng. **86**, 885 (2009).
[4] I. Mizushima, T. Sato, S. Taniguchi, and Y. Tsunashima, Appl. Phys. Lett. **77**, 3290 (2000).
[5] M.-C. M. Lee, W.-C. Chiu, T.-M. Yang, and C.-H. Chen, Appl. Phys. Lett. **91**, 191114 (2007).
[6] J. Nakamura, K. Sudoh, and H. Iwasaki, Jpn. J. Appl. Phys. **46**, 7194 (2007).
[7] R. Malshe, M. D. Ediger, L. Yu, and J. J. de Pablo, J. Chem. Phys. **134**, 194704 (2011).
[8] H. P. Bonzel and E. Preuss, Surf. Sci. **336**, 209 (1995).
[9] P. C. dos Santos Claro, M. F. Castez, P. L. Schilardi, N. B. Luque, E. P. M. Leiva, and R. C. Salvarezza, ACS Nano **2**, 2531 (2008).
[10] K. Sudoh, H. Iwasaki, R. Hiruta, H. Kuribayashi, and R. Shimizu, J. Appl. Phys. **105**, 083536 (2009).
[11] K. Sudoh, H. Iwasaki, H. Kuribayashi, R. Hiruta, and R. Shimizu, Jpn. J. Appl. Phys. **43**, 5937 (2004).
[12] W. W. Mullins, J. Appl. Phys. **28**, 333 (1957).
[13] W. W. Mullins, J. Appl. Phys. **30**, 77 (1959).
[14] Under our assumption concerning the isotropic nature of the sample, the K coefficient is independent of the orientation. Although this assumption is not suitable for monocrystals, in the case of polycrystalline samples at moderately high temperatures, the mesoscopic coefficient K usually exhibits a rather weak dependence on the orientation.
[15] L. B. Leopold and W. B. Langbein, Sci. Am. **214**, 60 (1966).
[16] U. F. Mayer, J. Comput. Appl. Math. **20**, 361 (2001).
[17] A quantitative estimation of this transient time is given below in the present section.
[18] M. Abramowitz and I. A. Stegun, *Handbook of Mathematical Functions,* 10th ed. (Dover, New York, 1972), p. 361.
[19] For the sake of simplicity, we are introducing a dimensionless timelike variable $\tau = K(\frac{2\pi}{\lambda_x})^4 t$. Expressing our results in terms of τ, it remains valid irrespective of the specific value of the coefficient K.
[20] The superindex in $\mathcal{C}^{(a)}$ is used to stress the fact that Eq. (14) gives the curvature of the two-component approximation and not the corresponding "real" simulated interface.
[21] S. Asvadurov, B. D. Coleman, R. S. Falk, and M. Moakher, Phys. D **121**, 263 (1998).
[22] Notice that when $A_2 \to 0$, it would be expectable that theoretical curves merge smoothly with the theoretical expectations for peak-valley symmetric sine-generated solutions discussed in [28], which exhibit excellent agreement with numerical results for $A_1 = 1.5$ and $A_2 = 0$.
[23] Trajectories on the (A_1, A_2) plane related to rectangular initial conditions were obtained through the numerical computation of the Fourier coefficients of the function $\theta(s)$. The contribution of high-order harmonics is non-negligible in the initial stage of the evolution (as could be seen in Fig. 2); therefore the explicit comparison with trajectories related to 2CSGC is performed once such an initial stage has ended; in this situation, the spectral content is (approximately) embedded on the (A_1, A_2) plane.

[24] M. F. Castez and R. C. Salvarezza, Appl. Phys. Lett. **94**, 053103 (2009).
[25] M. F. Castez, P. C. dos Santos Claro, P. L. Schilardi, G. Andreasen, and R. C. Salvarezza, J. Phys. Chem. C **114**, 4603 (2010).
[26] M. F. Castez, J. Phys. Condens. Matter **22**, 345007 (2010).
[27] M. F. Castez, R. C. Salvarezza, J. Nakamura, and K. Sudoh, Appl. Phys. Lett. **97**, 123104 (2010).
[28] M. A. Madrid, R. C. Salvarezza, and M. F. Castez, J. Phys. Condens. Matter **24**, 015001 (2012).